Short Communication

I·M3 Institute of Materials, Minerals & Mining

Materials Science and Technology
1–6

DOI: 10.1177/02670836241235847
journals.sagepub.com/home/mst


Laser butt welding of AA7075 aluminium alloy and Ti6Al4V titanium alloy using a Cu interlayer

Asim Iltaf[1], Shayan Dehghan[1], Noureddine Barka[1] and Claude Belzile[2]

Abstract

Laser welding of AA7075 and Ti6Al4V, two very different aerospace alloys, was performed with a copper (Cu) interlayer to avoid the brittle Ti–Al intermetallics. The joint was formed owing to the diffusion of Cu into the AA7075 alloy and limited diffusion in Ti6Al4V alloy, followed by eutectic formation at the AA7075/Cu interface. Microstructural and energy dispersive spectroscopy (EDS) analyses of the joint area revealed the presence of eutectic phases at grain boundaries inside the AA7075 fusion zone (FZ). An interfacial Cu_3Ti_2 phase formed at the solid-state Ti6Al4V/Cu interface. A robust and sound joint was achieved through the effective utilisation of Cu as an interlayer.

Keywords

Dissimilar joint, microstructure, tensile strength, EDS, microhardness, interlayer

Received: 27 December 2023; accepted: 11 February 2024

Introduction

Lightweight, but most importantly durable materials are the key to reaching the goals, of hybrid structures, in terms of energy and fuel consumption for various industries such as automotive and aerospace.[1] Using lightweight dissimilar structures can significantly reduce the total weight of the structures and pollutant emissions.[2] Aluminium (Al) and titanium (Ti) are ideal for manufacturing lightweight vehicle structures, reducing fuel consumption and improving safety.[3,4] The aerospace industry benefits from their synergistic combination. The formation of brittle intermetallic compounds (IMCs) makes it difficult to weld Al–Ti and develop high-performance composite structures.[5] Few studies have investigated the laser welding of titanium alloys with 7000 series aluminium alloys[1,6,7]

Utilising an interlayer in welding effectively reduces IMC formation, improving joint performance as shown by Teshome et al.[8] Common interlayers encompass Ni, Cu, Mg, V and Ag/Ti-based filler metals.[9] Forming a solid solution with metals like Nb, V, Zr and Ta helps prevent brittle intermetallics. Additionally, substituting brittle Ti–Fe intermetallics with other types further improves joint performance.[10]

Laser welding is crucial for its ability to provide high precision, controlled welding with minimal heat input, resulting in strong, high-quality joints with less distortion. It is also versatile and capable of joining a wide range of materials, even those considered difficult to weld using traditional methods.[11,12] In this study, laser welding in butt configuration was used to join AA7075 and Ti6Al4V alloys, with a Cu interlayer. Notably, there has been limited research on the utilisation of a copper interlayer for laser welding of these alloys previously. The results of this investigation are expected to improve the understanding of laser welding of Al and Ti alloys and make way for more widespread use of dissimilar material welding in the industry[11,12]

Experimental procedure

The present study used AA7075 aluminium alloy and Ti6Al4V titanium alloy sheets (80 mm × 50 mm × 1.6 mm).

[1]Department of Mathematics, Computer Science and Engineering, University of Quebec at Rimouski, Rimouski, Quebec, Canada
[2]Institute of Marine Sciences of Rimouski, University of Quebec at Rimouski, Rimouski, Quebec, Canada

Corresponding authors:
Asim Iltaf, Department of Mathematics, Computer Science and Engineering, University of Quebec at Rimouski, Rimouski, Quebec G5L 3A1, Canada.
Email: asim.iltaf@uqar.ca

Shayan Dehghan, Department of Mathematics, Computer Science and Engineering, University of Quebec at Rimouski, Rimouski, Quebec G5L 3A1, Canada.
Email: shayan.dehghan@uqar.ca

A Cu interlayer (99.95% purity) of 0.4 mm thickness was inserted between the two alloys to reduce the formation of IMCs. The oxide coating and greasy dirt on the surface of both alloys were cleaned off using SiC sandpaper and acetone before welding. Weld parameters were optimised with the Cu interlayer before the experiment was carried out. Consequently, AA7075 alloy and Ti6Al4V alloy were joined using an optimised set of process parameters, which included a laser power of 3 kW, a scanning speed of 40 mm/s and a laser spot size of 1.5 mm. The welding was performed in butt configuration using a fiber laser equipped with an IPG Photonics Ytterbium Laser Systems source model (YLS-3000-ST2) and the laser was pointed toward the weld centerline as shown in Figure 1(a). The resultant weldment was etched by Kroll solution (6% HNO_3 and 2% HF by volume in distilled water) to reveal the microstructure. The etching time was reduced for the dissimilar joint to avoid over-etching/over-corrosion as compared to the etching of base alloys. The etching time for base alloys was approximately 25–30 seconds while for the joint area it was around 10–15 seconds. The joint area was protected with hot glue while etching the base alloys. The nanoindentation test was performed in load control mode having a peak load of 200 mN using the Nanoindenter (iMicro from Nanomechanics, Inc.) with a Berkovich indenter tip. Scanning electron microscope (SEM) (SNE-4500M Plus, SEC) equipped with an energy dispersive spectroscopy (EDS) detector (Esprit, Bruker) was used to study fractography and chemical composition of the joint and fractured surface.

Results and discussion

Figure 1 shows the cross-sectional microstructure of the dissimilar butt joint of AA7075 and Ti6Al4V made by laser welding using Cu as an interlayer. The joint consists of three regions of interest: AA7075 fusion zone (FZ), mix zone and Ti6Al4V/Cu interface. There is minimal melting phenomena of the titanium alloy, and the joint interface is flat.[13] Minimising the melting of titanium during welding is crucial as it reduces the mixing of titanium atoms with aluminium atoms, thereby significantly lowering the likelihood of forming a brittle Ti/Al intermetallic compound. This preservation of the base materials' properties results in a stronger, more ductile weld joint, maintaining the integrity and performance of the base materials. Therefore, the interaction between the AA7075 and Cu and Ti6Al4V and Cu was the focus of the present investigation. The joint was mainly formed at the AA7075/Cu and Ti6Al4V/Cu interface owing to the eutectic liquid forming and limited diffusion of Cu into Ti6Al4V, respectively. Cu diffused into the AA7075 alloy, resulting in the formation of a large diffusion zone inside the AA7075 alloy and adjacent to the mix zone (Figure 1(b)-I, II). Some discontinuous minor cracks can be observed inside the AA7075 FZ (Figure 1(b)-II). The minimal effect of the current process on the Ti6Al4V can also be observed in Figure 1((b)-III). In laser beam welding (LBW), a rapid cooling rate results in significant local undercooling.[14] This phenomenon promotes faster nucleation and development of fine grains and dendrites as shown in Figure 1(b)-IV, V. The mix zone mainly consists of AA7075, Ti6Al4V and Cu (Figure 1(b)-VI). In the mix zone, a vanadium solid solution was formed and this led to a more robust joint. Vanadium solid solution contributes to strengthening mechanisms in several ways. Firstly, it can create a size mismatch due to its distinct atomic size, which generates lattice distortions and thus impedes the movement of dislocations in the material. This resistance to dislocation motion enhances the strength of the alloy. Additionally, the presence of vanadium can also lead to the formation of secondary phases or precipitates which can further obstruct dislocation movement, contributing to the overall strengthening effect. These mechanisms make vanadium a valuable element in alloy design for improved mechanical properties.

Figure 1(b) also shows the presence of porosity in the joint. Pore formation is a significant issue in LBW of 7xxx series alloys. This occurs due to a small amount of gas getting into the laser-melted zone, leading to gas porosity. Hydrogen (H_2), which has a high solubility in molten aluminium, is the primary cause of pore formation in this alloy. The hydrogen originates from oxides or impurities in the filler and base materials, which then dissolve into the bulk material.[15] On the other hand, porosity in LBW occurs in various forms, including necking, swelling and collapsing. The primary cause of porosities is the inconsistent vapourisation of volatile alloying elements like Zn and Mg, which have varying vapour pressures.[15]

SEM images of the unetched joint along with some points in AA7075 FZ for EDS analysis are presented in Figure 2((a)-I, II). EDS mapping showed a higher concentration for Cu in the AA7075 FZ interface, indicating the slow diffusion of Cu out of the mix zone (Figure 2(a)-III). The initial stage of the joining procedure was the process of diffusion, Cu was diffused into the AA7075. Afterward, the eutectic liquid is formed consisting of Al and Cu at the bonding temperature, as determined by the AA7075–Cu phase diagram.[16] Grain coarsening can also be observed near the AA7075/Cu interface. There were three primary eutectic phases present at the interface of the joint in AA707/5 FZ; Al_2Cu, $Al_{13}Fe$ and $Al_2Mg_3Zn_3$ (Figure 2(a)-IV, V). The Al–Cu phase diagram also allows for the prediction of the formation of Al_2Cu and $Al_{13}Fe$ at the interface region of the weldment.[16] Whereas, $Al_2Mg_3Zn_3$ is potentially formed by the solidification of the eutectic liquid during the cooling process (referred to Table 1). As the Al_2Cu phase excluded Mg and Zn throughout its growth, it led to the formation of $Al_2Mg_3Zn_3$ near the Al_2Cu phase in the AA7075 FZ.

The EDS analysis presented in Table 1 reveals the absence of Ti in the eutectic phases located at the AA7075 FZ, that is Al_2Cu, $Al_{13}Fe$ and $Al_2Mg_3Zn_3$. The concentration of Cu, Mg and Zn is significantly higher in AA7075 FZ as compared to Ti6Al4V. However, the EDS analysis also showed the diffusion of Cu into the Ti6Al4V. The Cu mapping in Figure 2(a-III), obtained from the joint, exhibits a prominent Cu concentration towards the Ti6Al4V interface as well. The presence of Cu at the Ti6Al4V/Cu interface indicates the formation of

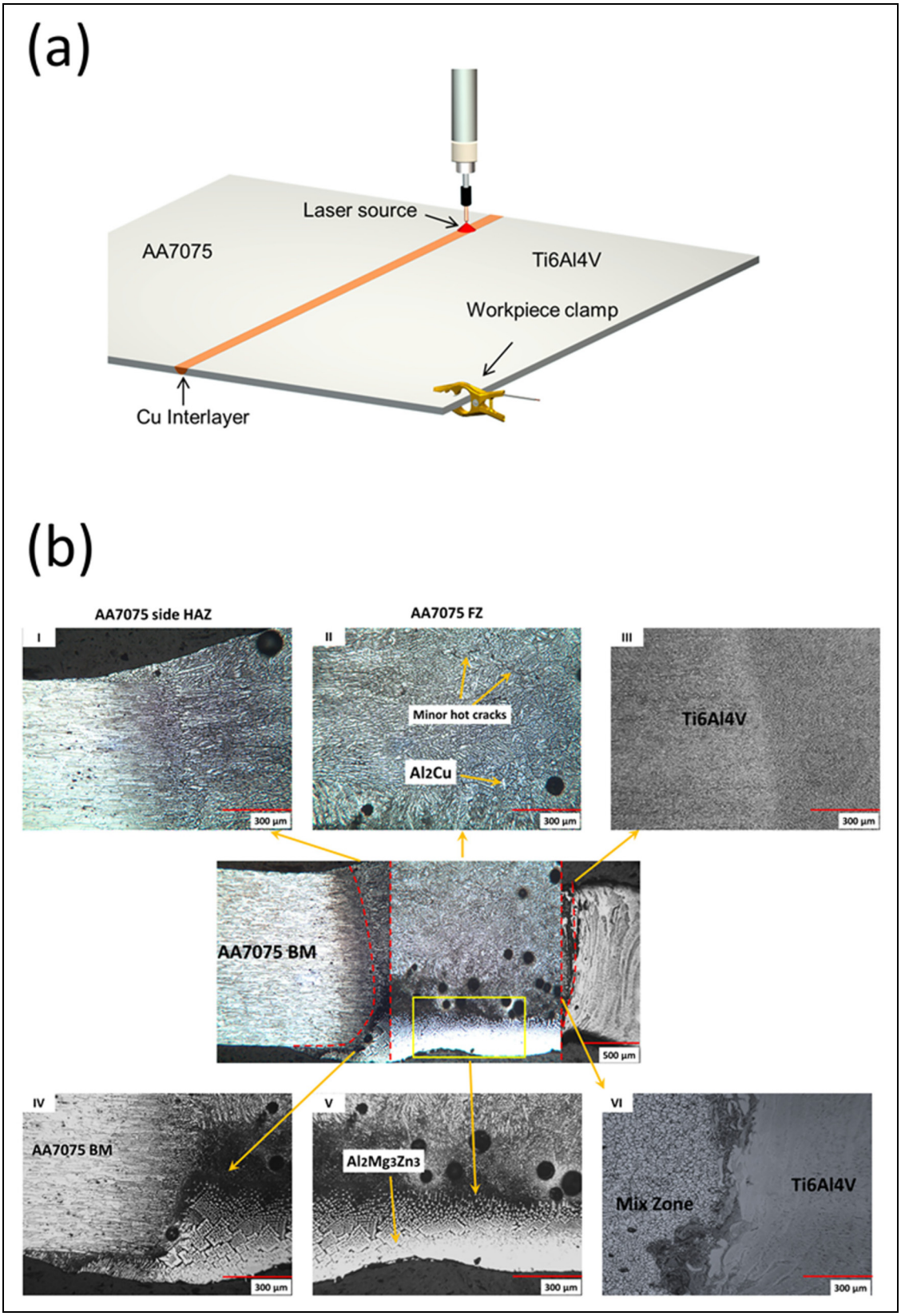

Figure 1. (a) Schematic diagram of laser welding in butt configuration; (b) microstructural evolution of dissimilar joint of AA7075–Ti6Al4V with Cu interlayer.

the Cu_3Ti_2 phase. Consequently, a solid-state bond was formed at the Ti6Al4V/Cu interface owing to Cu_3Ti_2. Figure 2(b) shows the microhardness profile over the joint region. Hardness values were found to increase from AA7075 FZ to the mix zone and Ti6Al4V. Owing to the formation of the Cu_3Ti_2 phase at the Ti6Al4V/Cu, higher

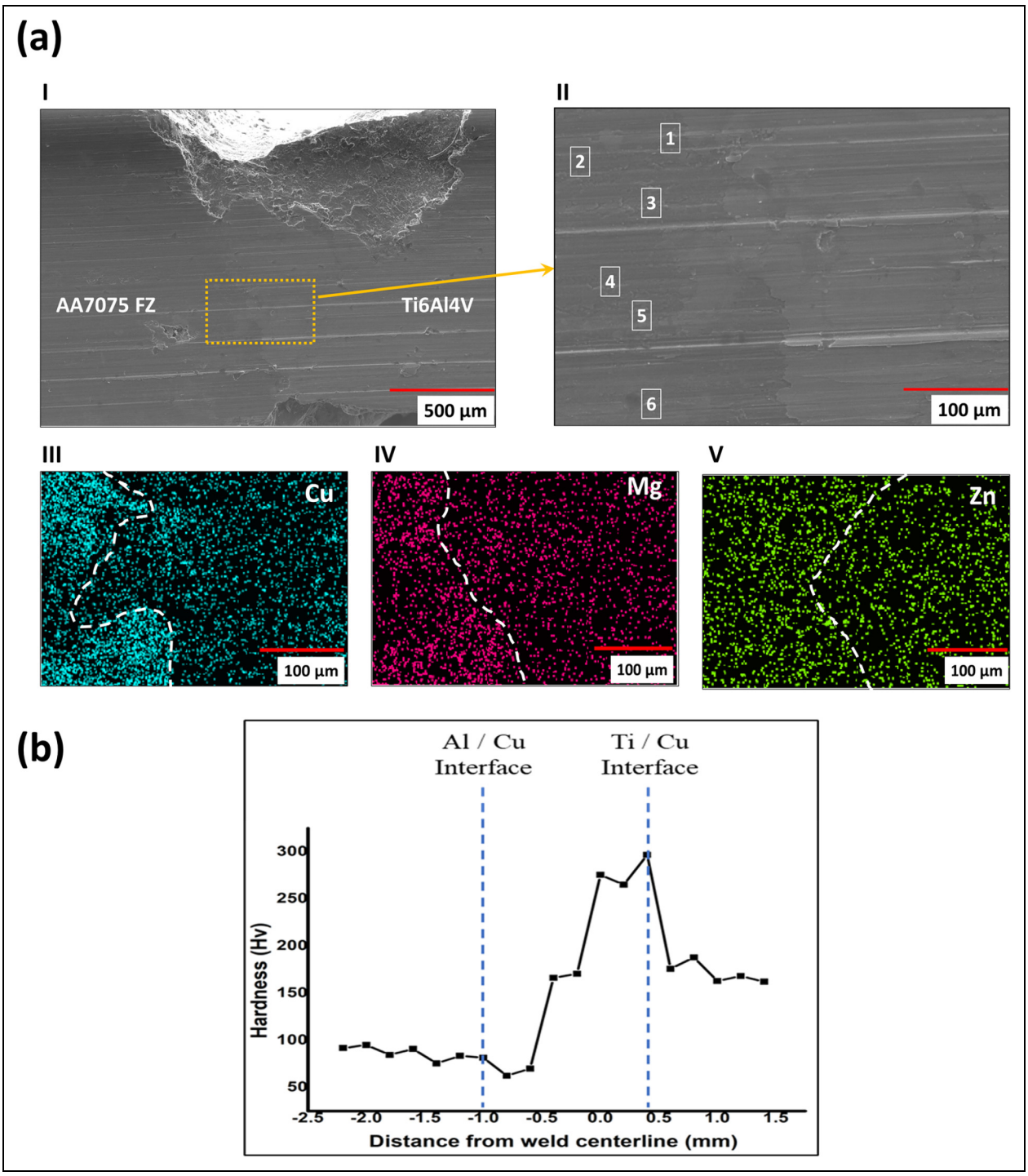

Figure 2. (a-I) SEM image of the joint without etching; (a-II) selected points of interest for EDS and the results are shown in Table 1; (a-III, IV and V) elemental mapping of Cu, Mg and Zn; (b) microhardness profile starting at Ti6Al4V/Cu interface.

Table 1. Chemical composition of the different regions (Figure 2) as measured by EDS (at.-%).

Spectrum no.	Al	Ti	Zn	V	Fe	Ni	Cu	Mg	Sn	Potential phases
1	Bal.	1.03	0.58	1.20	0.51	0.04	30.24	0.37	0.33	Al_2Cu
2	Bal.	0.06	0.41	0.38	7.68	0.03	25.84	0.16	0.09	$Al_{13}Fe + L$
3	Bal.	0.30	1.18	0.03	0.66	0.04	41.33	0.01	0.05	Al_2Cu
4	Bal.	0.08	8.37	0.01	0.27	0.08	18.30	0.21	0.01	$Al_2Mg_3Zn_3$
5	Bal.	0.60	1.47	0.05	0.60	0.06	43.26	2.31	0.07	Al_2Cu

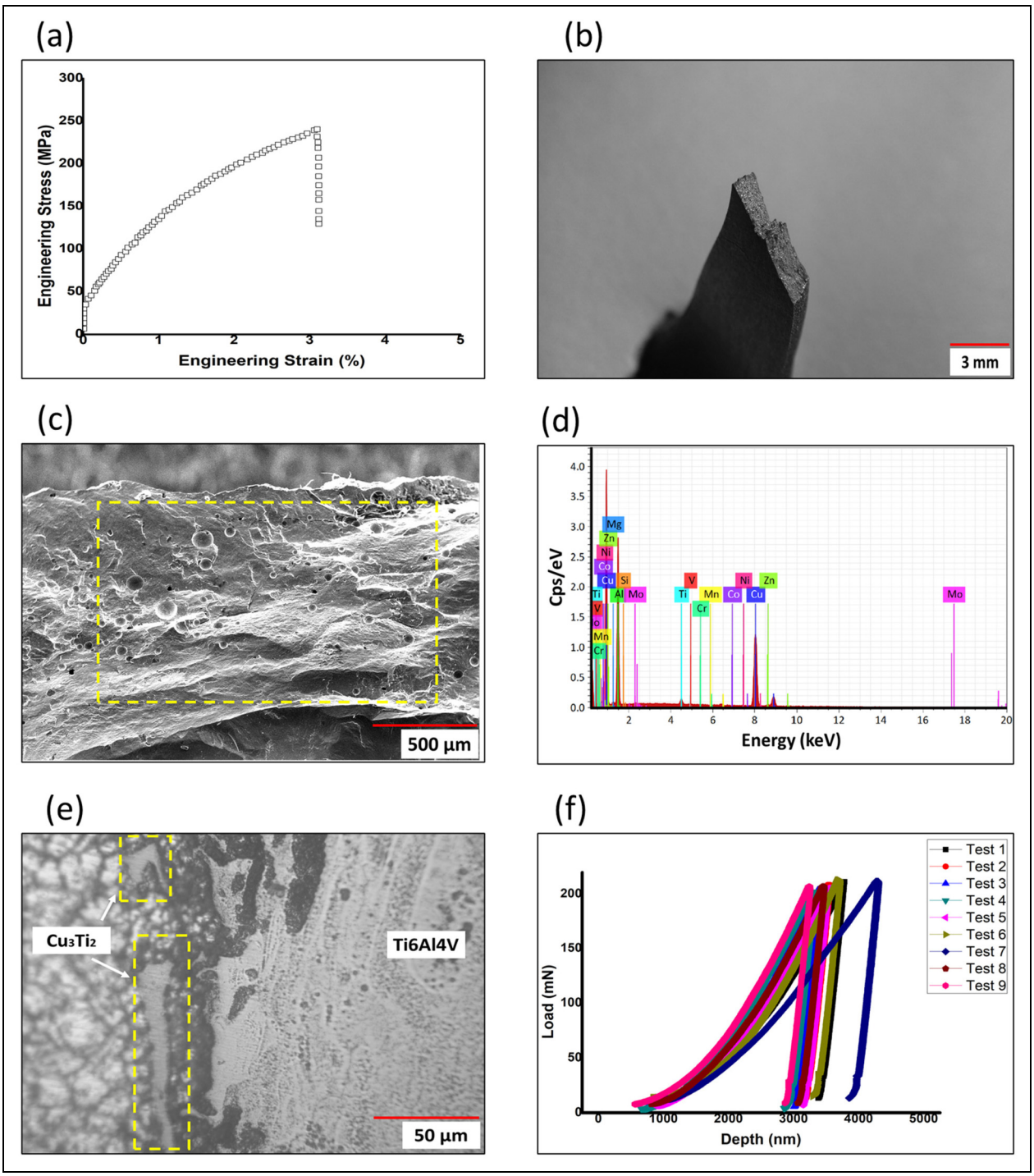

Figure 3. (a) Tensile test curve; (b) physical appearance of the fractured tensile specimen; (c) SEM image of fractured surface; (d) EDS spectra of fractured surface; (e) fracture location; (f) *P–h* curves across AA7075 FZ, mix zone and Ti6Al4V/Cu interface.

Table 2. Chemical composition of the fractured surface (Figure 3(c)) as measured by EDS (at.-%).

Spectrum no.	Ti	Al	V	Fe	Zn	Mg	Ni	Cu	Potential phases
1	42.47	2.25	0.44	0.95	0.84	0.13	0.67	Bal.	Cu_3Ti_2

hardness is indicated at this interface. While the formation of the Cu_3Ti_2 interfacial phase can enhance joint strength, it can also introduce brittleness. IMCs are often more brittle than base materials, which can lead to cracking under stress or impact, especially in applications where the weld is subject to dynamic loading or thermal cycling. Therefore, the formation of the Cu_3Ti_2 phase resulted in high high-strength Ti6Al4V/Cu interface while reducing

the ductility and toughness of the weld joint, making it less able to absorb energy and more susceptible to brittle fracture.

The weld's tensile strength was measured and the results are shown in Figure 3(a). Three tensile specimens were tested to ensure the repeatability and reliability of the results. Three samples were used to confirm that the observed mechanical properties are consistent and not an anomaly of a single specimen. The UTS was observed to be at 240 MPa. The test was repeated thrice, every sample examined fractured at the Ti6Al4V/Cu alloy interface, suggesting that the Ti/Cu alloy interface was the weakest point in the weldment. Following the tensile test, the fractured surface was analysed as shown in Figure 3(b), (c), which exhibits a brittle cleavage fracture mechanism. Figure 3(c) shows the cleavage plane, as well as the steps and black blocky substances. Moreover, Figure 3(c) demonstrates that the fracture surface is lumpy and uneven due to the extraction of several second phases. EDS spectra of the fractured surface indicate prominent peaks of Ti and Cu signifying the presence of Cu_3Ti_2 IMCs as shown in Figure 3(d) and Table 2. Stress concentrations due to the formation of Cu_3Ti_2 near the Ti6Al4V/Cu interface are primarily responsible for the joint's fracture (Figure 3(e)). The Cu_3Ti_2 near the weld toe probably interacted with the stress concentrations to cause the fracture. Furthermore, nanoindentation was conducted in a 3×3 grid across the AA7075FZ, mix zone and Ti6Al4V/Cu interface, and the load–displacement (P–h) curves of the various zones are shown in Figure 3(f). The nanoindentation results were consistent with the EDS analysis and microhardness results above. Ti6Al4V/Cu interface showed lower penetration depth (Test 9) among all the regions validating the presence of brittle Cu_3Ti_2.

Conclusion

This research explored the use of Cu as an interlayer for laser welding AA7075 and Ti6Al4V alloys. Following conclusions are drawn from this study:

- Utilising copper as an interlayer in laser welding led to successful dissimilar joining between AA7075 and Ti6Al4V alloys.
- Owing to the formation of eutectic phases such as Al_2Cu, $Al_2Mg_3Zn_3$ and $Al_{13}Fe$ in the FZ of AA7075, the brittleness of the joint was reduced. On the other hand, diffusion of Cu into Ti6Al4V resulted in a brittle Cu_3Ti_2 IMC at the Ti6Al4V/Cu interface.
- Tensile test result showed that the joint achieved an approximate tensile strength of 240 MPa.
- EDS analysis of the fractured tensile specimens indicated that the fracture occurred due to the formation of Cu_3Ti_2 at the Ti6Al4V/Cu interface.
- The microhardness and nanoindentation tests further validated the EDS analysis, confirming the observations.

Declaration of conflicting interests

The authors declared no potential conflicts of interest with respect to the research, authorship and/or publication of this article.

Funding

The authors received no financial support for the research, authorship and/or publication of this article.

References

1. Liu S, Chew Y, Weng F, et al. Effects of laser pulse modulation on intermetallic compounds formation for welding of Ti–6Al–4V and AA7075 using AA4047 filler. *Mater Des* 2022; 213: 110325.
2. Gagliardi F, Palaia D and Ambrogio G. Energy consumption and CO2 emissions of joining processes for manufacturing hybrid structures. *J Clean Prod* 2019; 228: 425–436.
3. Fernandes FAO, Gonçalves JJM and Pereira AB. Evaluation of laser lap weldability between the titanium alloy Ti–6Al–4V and aluminum alloy 6060-T6. *Crystals (Basel)* 2023; 13: 1448.
4. Anchev A, Kaisheva D, Kotlarski G, et al. Welding of Ti6Al4V and Al6082-T6 alloys by a scanning electron beam. *Metals (Basel)* 2023; 13: 1252.
5. Dak G and Pandey C. A critical review on dissimilar welds joint between martensitic and austenitic steel for power plant application. *J Manuf Process* 2020; 58: 377–406.
6. Chen X, Lei Z, Chen Y, et al. Enhanced wetting behavior using femtosecond laser-textured surface in laser welding-brazing of Ti/Al butt joint. *Opt Laser Technol* 2021; 142: 107212.
7. Kuryntsev S V. Microstructure, mechanical and electrical properties of laser-welded overlap joint of CP Ti and AA2024. *Opt Lasers Eng* 2019; 112: 77–86.
8. Teshome FB, Peng B, Oliveira JP, et al. Role of Pd interlayer on NiTi to Ti6Al4V laser welded joints: microstructural evolution and strengthening mechanisms. *Mater Des* 2023; 228: 111845.
9. Zhang Y, Bi YB, Zhou JP, et al. Butt laser welding of TC4 titanium alloy and 304 stainless steel with Ag-base filler metal based on a hybrid connection mechanism. *Opt Laser Technol* 2020; 124: 105957.
10. Li J, Hu D, Mu G, et al. Optimal control strategy for large-scale VRB energy storage auxiliary power system in peak shaving. *Int J Electr Power Energy Syst* 2020; 120: 106007.
11. Ke W, Zeng Z, Oliveira JP, et al. Heat transfer and melt flow of keyhole, transition and conduction modes in laser beam oscillating welding. *Int J Heat Mass Transf* 2023; 203: 123821.
12. Zheng M, Yang J, Xu J, et al. Interfacial microstructure and strengthening mechanism of dissimilar laser al/steel joint via a porous high entropy alloy coating. *J Mater Res Technol* 2023; 23: 3997–4011.
13. Moon S, Paek JH, Jang YH, et al. Mixing behavior of Ti–Al interface during the ultrasonic welding process and its welding strength: molecular dynamics study. *Heliyon* 2024: e25116. DOI:10.1016/j.heliyon.2024.e25116.
14. Sonar T, Balasubramanian V, Malarvizhi S, et al. An overview on welding of Inconel 718 alloy – effect of welding processes on microstructural evolution and mechanical properties of joints. *Mater Charact* 2021; 174: 110997.
15. Khalil AM, Loginova IS, Pozdniakov AV, et al. Evaluation of the microstructure and mechanical properties of a new modified cast and laser-melted AA7075 alloy. *Materials* 2019; 12: 3430.
16. Yan XY, Chang YA, Xie FY, et al. Calculated phase diagrams of aluminum alloys from binary Al–Cu to multicomponent commercial alloys. *J Alloys Compd* 2001; 320: 151–160.